Appl. Phys. B (2004)
DOI: 10.1007/s00340-004-1719-8

Applied Physics B
Lasers and Optics

F. MÜLLER[1,2,✉]
G. VON BASUM[3]
A. POPP[1,*]
D. HALMER[3]
P. HERING[3]
M. MÜRTZ[3]
F. KÜHNEMANN[1,**]
S. SCHILLER[2]

Long-term frequency stability and linewidth properties of continuous-wave pump-resonant optical parametric oscillators

[1] Institut für Angewandte Physik, Universität Bonn, Wegelerstr. 8, 53115 Bonn, Germany
[2] Institut für Experimentalphysik, Heinrich-Heine-Universität Düsseldorf, Universitätsstr. 1, 40225 Düsseldorf, Germany
[3] Institut für Lasermedizin, Heinrich-Heine-Universität Düsseldorf, Universitätsstr. 1, 40225 Düsseldorf, Germany

Received: 27 September 2004 /
Revised version: 18 November 2004
Published online: 21 December 2004 •

ABSTRACT We present a frequency stability and linewidth analysis of two different setups of continuous-wave pump and signal-resonant optical parametric oscillators (pump resonant, singly resonant OPO, PR-SRO). Both designs, a common-cavity and a dual-cavity version, utilize a frequency-stable and narrow-linewidth pump laser and are stabilized without using an external reference. A long-term frequency stability better than ±30 MHz is reached over more than 30 minutes for both designs. The frequency jitter on a one-second time-scale is 56 kHz for the common-cavity PR-SRO and about 10 MHz for the dual-cavity PR-SRO. The short-term linewidths were measured using an external high-finesse cavity and are (9 ± 2)kHz and (6 ± 1)kHz in 20 μs, respectively. To our knowledge, these are the lowest values demonstrated so far for a widely continuously wavelength-tunable all-solid-state laser source.

PACS 42.65.Yj; 42.72.Ai; 42.62.Fi

1 Introduction

Continuous-wave optical parametric oscillators (cw-OPOs) [1, 2] have lately proved their usefulness as laser sources for spectroscopic applications, including quantum optics and trace gas analysis [3–13]. For the latter application, photoacoustic [4, 5, 14] and cavity leak-out spectroscopy (PAS, CALOS), a continuous-wave variant of cavity ring-down spectroscopy (CRDS) [4, 5, 15, 16], are established methods providing high sensitivity, selectivity and time resolution. For both techniques a widely tunable mid-infrared laser source is required for multigas analysis.

PAS, which operates at atmospheric pressure, puts the weakest requirements on the linewidth of the radiation source, since multiple lines of a molecular absorption band form GHz-wide structures. Stringent requirements on the spectral properties of cw-OPOs arise in quantum optics, CALOS and high-resolution spectroscopy on ultra-cold atoms and molecules [17]. In the latter, pressure broadening is absent and the transition linewidths can be lifetime-limited, in the range from tens of Hz to sub-Hz. To achieve an OPO linewidth at this level, an active stabilization is required [18]. A narrow free-running OPO linewidth (below 100 kHz) is a favourable starting point.

In some CALOS trace gas measurements, one operates with low gas pressures in order to improve selectivity by reducing cross-interference, often resulting in typically Doppler-broadened (∼100 MHz) molecular absorption linewidths. As an example, Fig. 1 shows the ${}^{p}Q_1$ subbranch of ethane whose linewidth is reduced from 5 GHz at atmospheric pressure down to 375 MHz at a pressure of 20 mbar. However, the relevant linewidth scale is determined by the leak-out cavity (LOC) linewidth on the order of 20 kHz. Such low values ensure a long decay time and thus a high detection sensitivity. However, an effective excitation of the cavity requires a source with a comparable linewidth. Since in CALOS the cavity excitation needs to last only a time comparable to the decay time, the OPO linewidth requirements needs only to

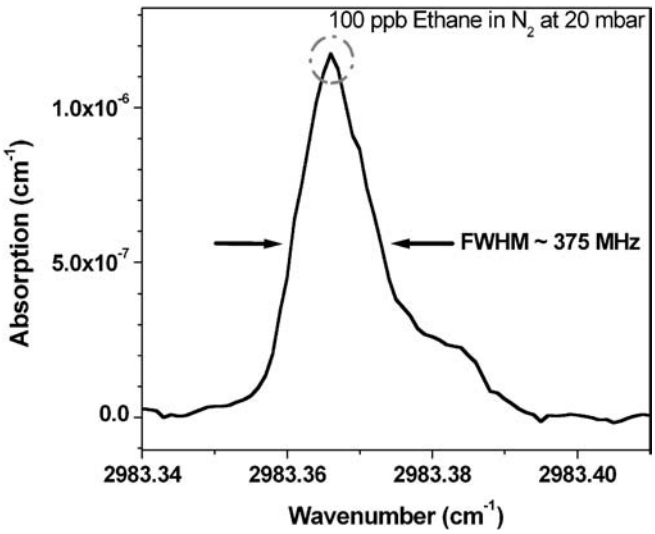

FIGURE 1 An ethane absorption structure at 20 mbar pressure obtained using CALOS and a dual-cavity PR-SRO. The *gray circle* marks the wavelength which is used for ethane monitoring

✉ Fax: +49-211-81-13116, E-mail: f.mueller@iap.uni-bonn.de
**Present address*: Medizinische Fakultät, TU Dresden, Fetscherstr. 74, 01307 Dresden, Germany
***Present address*: German University in Cairo, Dept. of Physics, New Cairo City, Egypt

be satisfied on a timescale of tens of μs. Trace gas detection usually implies the need for long-term measurements, e.g., in monitoring. Therefore, the laser source needs to be long-term frequency-stable to a level where the same absorption structure can be interrogated as long as desired, i.e., on the order of tens of MHz over minutes to hours.

With certain laser sources, these levels of linewidth and frequency stability in the order of tens of MHz over minutes to hours can only be achieved with significant effort, i.e., using active frequency stabilization, usually to a reference cell containing the gas to be monitored. Clearly, this approach becomes cumbersome in multi-species monitoring.

In this work we show that two cw-OPO types satisfy the above requirements for CALOS without any external stabilization and so are advantageous for this application. At the same time their properties make them suitable for high-resolution spectroscopy, where external stabilization cannot be avoided. Previously, linewidths of cw-OPOs have been measured by beating with narrow-linewidth lasers [9, 19] or by scanning slowly across a narrow-linewidth optical cavity [18]. Here we use, for the first time, the cavity ringing technique [20], which is both practical and accurate for determining linewidths on the μs timescale. The obtained values are below 10 kHz and are comparable to linewidths obtained from diode-pumped Nd:YAG lasers [21]. However, here such values are achieved for widely tunable sources.

2 Description of OPO systems

There are several designs of OPOs demonstrated in the literature. Singly resonant OPOs (signal or idler resonated) are the easiest in setup and application, but need high-power pump lasers to overcome the threshold [6–8, 22, 23]. Here we consider cw-OPOs using a pump source of moderate power. The necessary lowering of the pump threshold can be achieved by additionally resonating the pump or by resonating both generated waves. OPOs resonating signal and idler (doubly-resonant OPO, DRO) or all three waves (triply-resonant OPO, TRO) have been demonstrated with very low pump thresholds [18, 24–26]. The disadvantage of these systems is the complicated frequency stabilization and tuning. If a stable pump laser is used, a pump resonant, singly resonant OPO (PR-SRO) [9–13, 27–29] is a proven compromise between the easily stabilized SRO and the low threshold of DROs and TROs.

We have set up two different transportable versions of PR-SROs, each emitting up to 100 mW of idler power at each side of their cavities. Both use the same periodically poled lithium niobate (PPLN) crystal as the nonlinear medium. The crystal (Crystal Technology, length × width × thickness = 19 mm × 50 mm × 0.5 mm) contains 19 gratings with poling periods between 28.64 μm and 30.16 μm (poled by J.-P. Meyn) for quasi-phasematching (QPM). A 2.5 Watt cw Nd:YAG laser (Innolight Mephisto, linewidth ∼ 1 kHz/100 ms, frequency drift ∼ 1 MHz/min) at 1064 nm serves as the pump source. Coarse tuning of the idler wavelength in the range of 3.1–3.9 μm is performed by selecting between the 19 grating periods via a motorized translation stage and changing PPLN temperature between 150 and 200 °C. The input face of the crystal, where the beam waist (34 μm radius) is focussed on, serves as one cavity mirror for the pump (reflectivity $R = 94.3\%$) and signal ($R = 99.9\%$) waves. The second surface is antireflection coated for the three waves. In the first setup pump and signal wave are resonated in one common cavity (length ∼ 39 mm) closed by a meniscus mirror (M1, radius of curvature $r = 30$ mm, $R = 99.9\%$ for pump and signal), which is attached to a piezoelectric transducer (PZT) to change cavity length (Fig. 2). The free spectral range is 2.7 GHz. The cavity is locked to the laser via the Pound–Drever–Hall (PDH) method [30]. The pump laser is phase modulated at 6.48 MHz via its PZT. The beam reflected from the cavity is separated in the Faraday isolator and coupled into a photo detector. A generated error signal is fed to the servo regulating the OPO cavity PZT. The external pump threshold is 280 mW. An intrinsic advantage of the common-cavity design is the stabilization of the signal frequency to the pump frequency. Experience has shown, however, that the setup is very sensitive to mechanical vibrations, often resulting in mode-hops. Also, continuous frequency fine tuning by tuning the pump laser is strongly limited by spontaneous modehops, often preventing access to a desired frequency [10]. Inserting an etalon suppresses most of the spontaneous modehops [29], but the simultaneous resonance of two different wavelengths in one common-cavity is still a limitation for the frequency tunability.

These frequency tuning problems are solved by a linear dual-cavity setup [13, 28], where pump and signal waves are resonated in separate cavities (Fig. 3). The pump cavity (length ∼ 39 mm) is closed by a meniscus mirror (M1, $r = 30$ mm, $R = 99.9\%$ for pump), while the signal cavity (length ∼ 304 mm) is closed by a concave mirror (M2, $R = 99.9\%$ for signal, $r_{cav} = 450$ mm). Both mirrors are attached to respective PZTs to adjust the cavity lengths. The signal cavity has a free spectral range of 450 MHz. A galvanometer-mounted solid etalon (YAG, 0.5 mm, ∼ 50% signal reflectivity coating) is inserted into the signal cavity to suppress spontaneous mode-hops. The pump cavity is locked to the pump laser via the PDH method. The external pump threshold is 380 mW. Long-term frequency stability without mode-hops can be achieved over typically more than 30 minutes by sim-

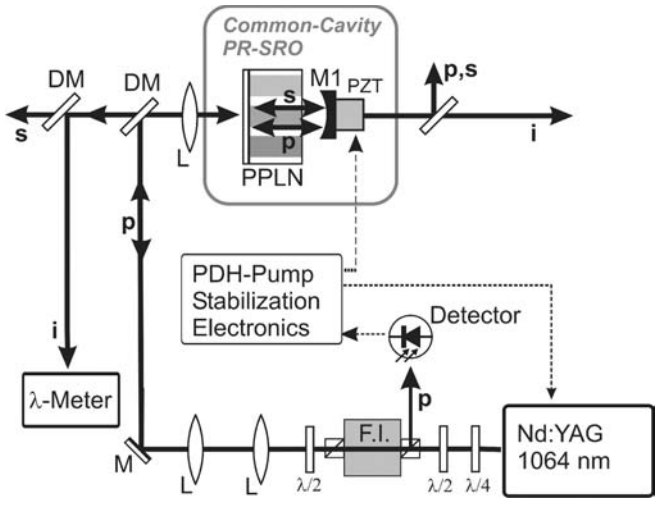

FIGURE 2 Common-cavity PR-SRO setup; M = mirror, DM = dichroic mirror, FI = Faraday isolator, L = lens, p = pump, s = signal, i = idler

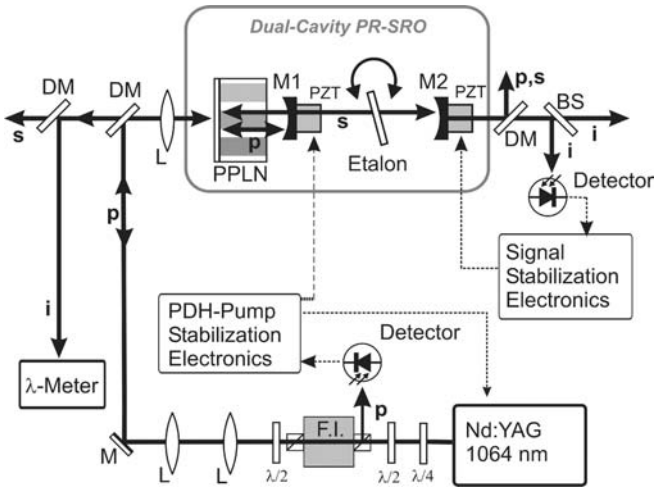

FIGURE 3 Dual-cavity PR-SRO; BS = beamsplitter

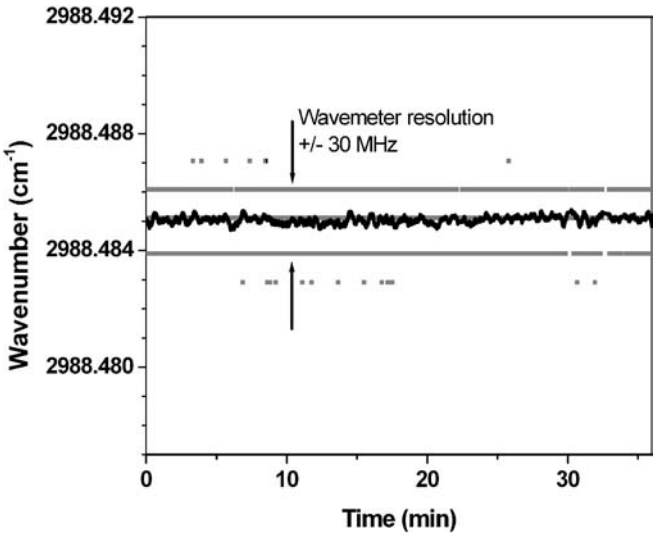

FIGURE 4 Long-term frequency stability (digital wavemeter read-out in 30 MHz steps and running average over 20 points) of the common-cavity PR-SRO

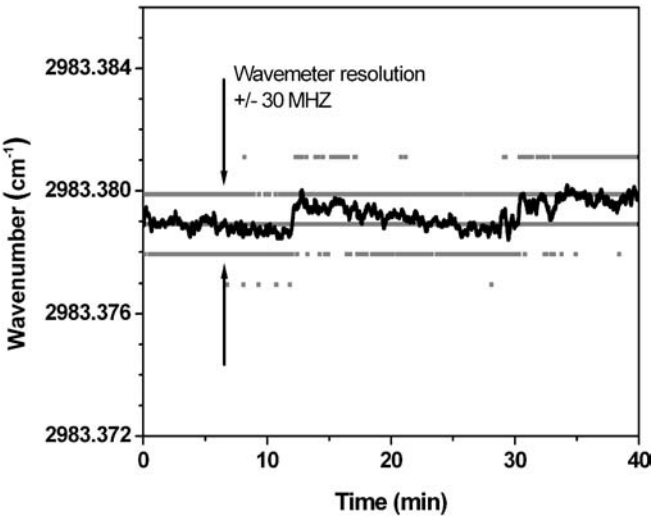

FIGURE 5 Long-term frequency stability (digital wavemeter read-out in 30 MHz steps and running average over 20 points) of the dual-cavity PR-SRO

ply locking the signal cavity to the point of maximum idler output power. For this purpose a frequency modulation signal with about 3 MHz amplitude at several hundred Hz is applied to the signal cavity PZT and synchronously detected. A stable idler frequency is thereby reached without using an external reference. Several options for frequency tuning are available, combining etalon, signal cavity and pump frequency tuning. The dual-cavity design also solves the problem of the strong tuning limitation due to spontaneous mode-hops. In the following the frequency stability and linewidth of both OPO designs are presented.

3 Experiment

3.1 *Long-term frequency stability*

For the analysis of long-term frequency stability the idler output frequency is measured with a wavemeter (Burleigh WA1500). The wavemeter digital read-out is in 30 MHz steps and the refresh-rate is one second. For both OPOs the measured frequency is more stable than the wavemeter resolution of ±30 MHz. A comparison of the running averages of the digital readouts shows differences between the two OPOs. For the common-cavity design the running average shows a constant frequency, whereas for the dual-cavity design a drift of about 30 MHz over a period of about 10 minutes followed by a 30 MHz hop is visible (Figs. 4, 5). The reason for these behaviours is the different methods used for the signal wave stabilization of the two OPOs. In the common-cavity PR-SRO the signal wave is strongly stabilized to the very stable pump laser frequency, and so the idler also has high frequency stability.

In the dual-cavity PR-SRO the signal cavity is stabilized to maximum idler output power and so the idler frequency is coupled to the frequency of the maximum of the gain curve. If the frequency of maximum gain shifts in the course of time, so will the signal and idler oscillation frequencies. The gain curve is obtained by measuring the dependence of idler power on idler frequency. With the available setup, information about the spectral dependence of the gain can only be obtained with the OPO oscillating stably and thus only a small region near the maximum of the etalon-dominated gain curve can be measured: it spans 450 MHz (1 signal cavity FSR) as compared to the etalon FSR of 37 GHz. This is shown in Figs. 6 and 7, which show the frequency dependence of idler power as a function of time, while the signal cavity length is scanned over several FSRs with the etalon angle fixed. Note that the idler power curve retraces itself after each signal mode-hop. The power variation is only about 10%. Under lock, the signal cavity length is stabilized to the point of maximum of idler emission power. It is therefore of interest to investigate the temporal variation of the shape of the emission curve, see Fig. 7.

The frequency-dependent structures in the idler power are reproducible to some extent over the timescale of minutes, but may strongly change over longer timescales (tens of minutes to hours), as seen in Fig. 7. Note that from the traces one cannot directly deduce the absolute shift in frequency of the maximum since the frequency of the modehop points can also shift in time. We believe that changes of

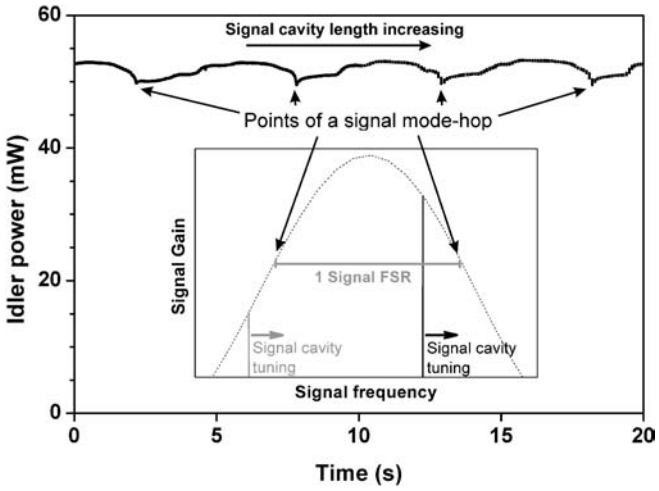

FIGURE 6 Idler power of the dual-cavity PR-SRO measured while scanning the signal cavity length linearly in time. At the marked times the signal frequency jumps by 1 FSR = 450 MHz, with a corresponding opposite idler frequency jump. In-between the marked times the signal and idler frequencies change linearly in time in opposite directions. The *inset* shows schematically the tuning process: By tuning the signal cavity length, the signal modes (*vertical lines*, the oscillating mode in *black*, the non-oscillating neighbour mode in *grey*) are moved with respect to the gain curve (shaped by the etalon Airy-function, *dotted grey line*). When the signal detuning reaches a certain value, a signal (and idler) mode-hop to the neighbour mode occurs

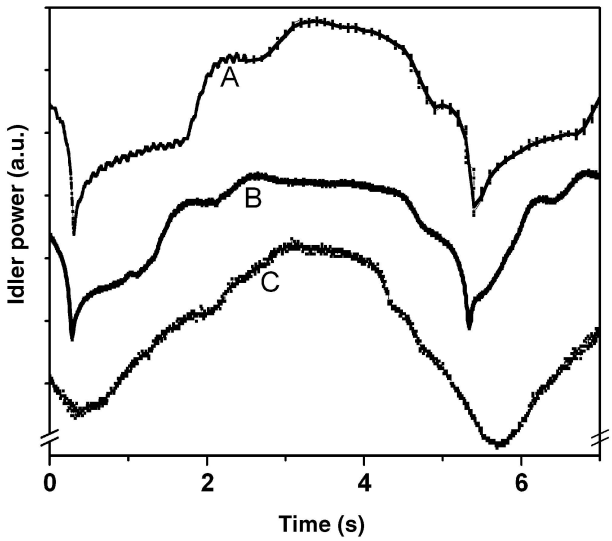

FIGURE 7 Idler power measured while scanning the signal cavity length linearly in time over a little more than one FSR. Note that the time span is much less than in Fig. 6. Vertical shifts are introduced for a better visibility. Scan A is measured about 4 minutes after scan B, both showing clear structures. Scan C was measured about an hour later, showing less pronounced structures. The curves were shifted horizontally so that the positions of the mode-hops coincide

the structures with time to be the reason for the observed slow frequency changes in Fig. 5. A quantitative analysis of these changes by assigning absolute frequency values to the time abscissa in Fig. 7 is not possible due to the slow refresh rate of the wavemeter. In contrast, for the common-cavity PR-SRO structures in the gain curve do not affect the idler emission frequency as the signal frequency (and therefore the idler frequency) is stabilized to the pump frequency.

3.2 *Short-term frequency fluctuations*

To measure the emission line profile on a shorter timescale, the leak-out cavity (LOC, length $l = 52.5$ cm, mirror reflectivity $R = 99.985\%$) of the CALOS setup is used as a high-resolution fixed-frequency interferometer (Fig. 8).

For our measurements with the common-cavity setup the idler frequency is swept across the LOC resonance using external modulation by means of an acousto-optic modulator (AOM) with the LOC length fixed. The sweep frequency was 90 Hz with an amplitude of 1 MHz. The transmitted signal is measured with an InSb photo-detector and recorded by a digital storage oscilloscope (Tektronix, 500 MHz/s maximum sampling rate). Averaging over 1.8 seconds, the envelope of this signal has a full width at half maximum (FWHM) of $\Delta\nu = 56$ kHz (Fig. 9). The measured width can be decomposed as $(\Delta\nu)^2 = (\Delta\nu_{\mathrm{OPO}})^2 + (\Delta\nu_{\mathrm{LOC}})^2$. With a LOC linewidth $\Delta\nu_{\mathrm{LOC}} = 12.4$ kHz, we obtain an OPO linewidth of $\Delta\nu_{\mathrm{OPO}} = 54.6$ kHz. As this value may contain a contribution from LOC length fluctuations, it represents an upper limit for the common-cavity PR-SRO linewidth. For a common-cavity PR-SRO with a kHz linewidth pump laser similar to ours,

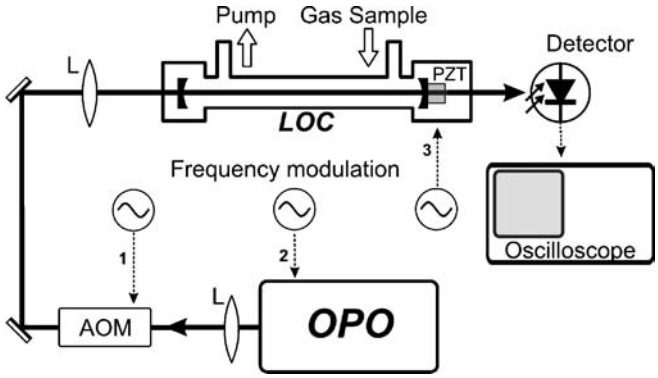

FIGURE 8 Linewidth characterization setup using a ring-down cell (LOC). The cell is empty. Overlap between OPO emission and LOC resonance can be achieved by frequency modulation of the idler wave via the AOM (1) or, in the dual-cavity PR-SRO system, by modulating the signal cavity length (2), or by modulating the LOC length (3)

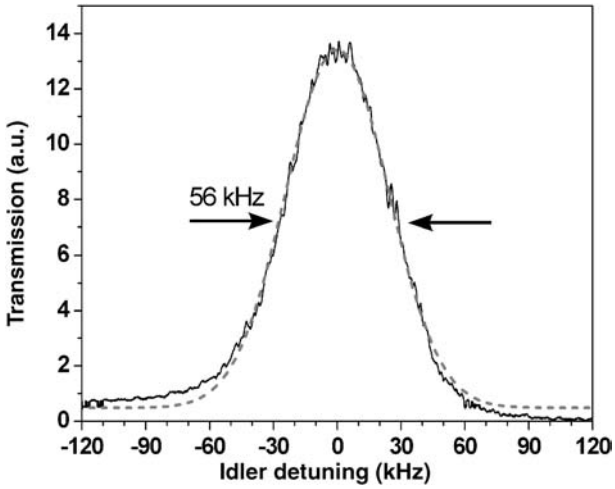

FIGURE 9 Transmission of the common-cavity PR-SRO idler wave through the fixed-frequency LOC (*solid line*). Averaging time is 1.8 seconds (120 scans). *Dashed line*: Gaussian fit

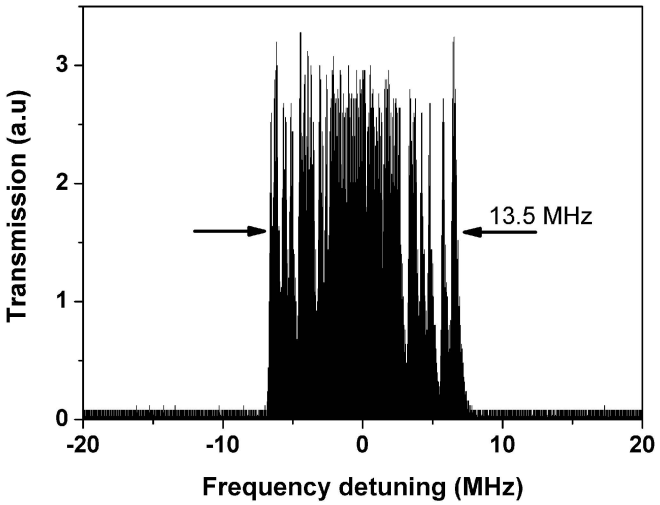

FIGURE 10 Transmission of dual-cavity PR-SRO idler radiation through the LOC, averaged over 1.5 seconds (100 scans)

Kovalchuk et al. [9] found a linewidth of the same order of magnitude ($\sim$ 100 kHz), but for an integration time several orders of magnitudes shorter (500 µs).

The same analysis was performed with the dual-cavity setup. Here the signal cavity was servo-stabilized (10 ms integration time) in the manner described above using a signal cavity modulation at 330 Hz and 3 MHz amplitude. Overlap between the LOC resonance and the PR-SRO emission is reached by sweeping the LOC frequency over about 300 MHz at 26 Hz. Averaging over 1.5 seconds, the envelope of the transmitted signal has typically a FWHM of 13.5 MHz, including the 6 MHz peak–peak signal frequency modulation (Fig. 10). Since we observed that the rectangular shape of this envelope is not due to a frequency jitter, the position of the gain maximum changed during the scanning time. Thus, the significant difference of the shapes for the two OPO setups lies in the different stabilization methods used. For comparison, the dual-cavity PR-SRO without signal cavity stabilization exhibits a somewhat larger jitter of 12–18 MHz.

3.3 *OPO linewidth*

Measurements with the LOC may also be used to determine the linewidth of the OPO on the µs timescale, where frequency fluctuations due to mechanical noise or temperature instability are negligible. When tuning the OPO idler frequency across the LOC resonance, the LOC transmission shows a characteristic ringing structure, provided the sweep time is much shorter than the decay time and the laser jitter is stochastic. The reason for this effect is the interference between the incoupled laser wave and the decaying light inside the resonator. The linewidth of the OPOs can be determined using the method of Li et al. [20]. In the following we use their notation. The effective input field including the stochastic laser jitter (second exponential term) can be modeled by

$$A_i(t) = A_0 \mathrm{e}^{\mathrm{i}\omega(t)t} \mathrm{e}^{-|t|\pi\Delta\nu_{\mathrm{OPO}}} \tag{1}$$

in the case of white frequency noise. The first exponential term describes a wave with constant amplitude A_0 and instantaneous angular frequency $\omega(t)$. The second real exponential term models stochastic frequency fluctuations with a white frequency noise spectrum. The power spectrum of this term is a lorentzian of FWHM OPO linewidth $\Delta\nu_{\mathrm{OPO}}$. The angular frequency can be expanded in a Taylor series in time around the value $\omega(t=0) = \omega_0$, the injected frequency, with the relative scanning rate (first derivative) and higher nonlinearities. The transmitted amplitude is given by the convolution of the LOC transfer function and the input field:

$$A_t(t) = C\mathrm{e}^{-\gamma_c t}\mathrm{e}^{\mathrm{i}\omega_0 t} \int_{-\infty}^{\gamma_c t} e^{\tau - b|\tau|} \mathrm{e}^{\mathrm{i}\tau^2(a_1 + a_2\tau + a_3\tau^2)}\,\mathrm{d}\tau \tag{2}$$

with the LOC linewidth

$$\gamma_c = \pi\Delta\nu_{\mathrm{LOC}} \quad , \tag{3}$$

the relative OPO linewidth

$$b = \frac{\Delta\nu_{\mathrm{OPO}}}{\Delta\nu_{\mathrm{LOC}}} \quad , \tag{4}$$

and the normalized Taylor expansion coefficients

$$a_1 = \frac{\dot{\omega}_0}{\gamma_c^2}, \quad a_2 = \frac{1}{2}\frac{\ddot{\omega}_0}{\gamma_c^3}, \quad a_3 = \frac{1}{6}\frac{\dddot{\omega}_0}{\gamma_c^4} \quad . \tag{5}$$

The change of variables is introduced for a better visibility of (2). The intensity $|A_t(t)|^2$ measured behind the LOC shows oscillations (ringing structures as described above) on the decay curve which are damped by the term including b in (2). Thus, the parameter b determines the contrast of the ringing, see Fig. 11. The LOC linewidth can be determined from the decay time of the ringing signal.

In the measurements with the common-cavity OPO, the frequency scan rate of the idler frequency was 12.57 kHz/µs using the AOM. The ringing signal was best fitted with $b = 0.7$ and a decay time $1/(2\gamma_c) = 12.8$ µs (Fig. 12). With a LOC linewidth $\Delta\nu_{\mathrm{LOC}} = 12.4$ kHz the common-cavity OPO linewidth is $\Delta\nu_{\mathrm{OPO}} = 8.7$ kHz in 20 µs.

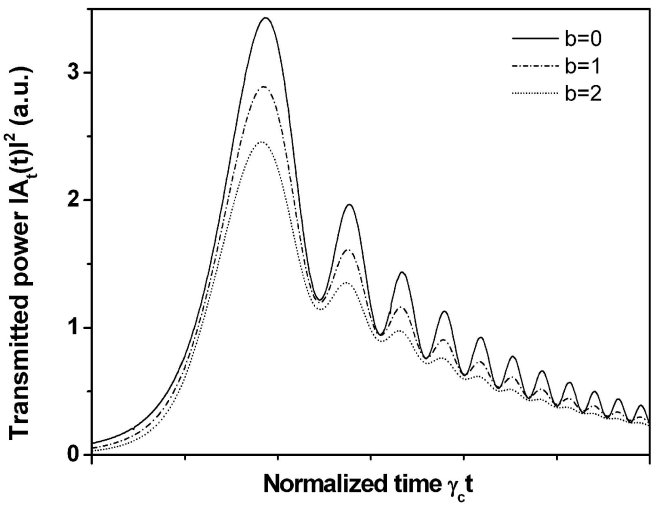

FIGURE 11 Theoretical dependence of the visibility of a ringing signal on the relative OPO linewidth b. In this plot $a_2 = 0$, $a_3 = 0$

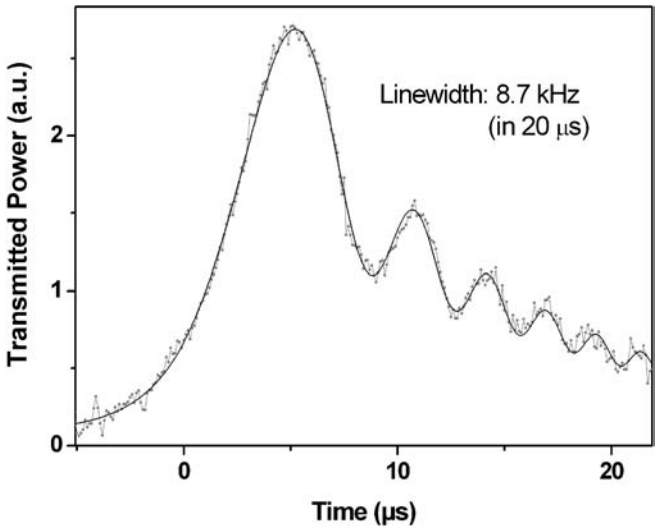

FIGURE 12 Measurement of the ringing signal (*dots*) and fit (*solid line*) for the common-cavity PR-SRO

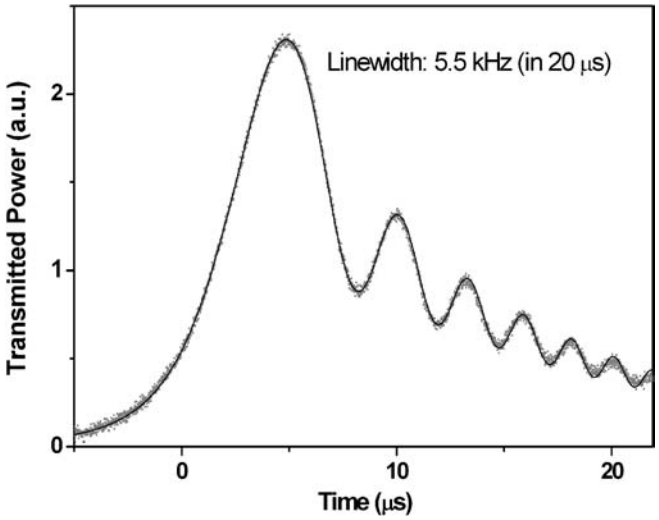

FIGURE 13 Measurement of the ringing signal (*dots*) and best fit (*solid line*) for the dual-cavity PR-SRO

The measurements with the dual-cavity OPO were performed with an idler frequency modulation over ± 3 MHz at a frequency of 702 Hz, resulting in a scanning speed of 13.28 kHz/μs. The decay time was $1/(2\gamma_c) = 11.6\,\mu$s. The ringing signal was best fitted with $b = 0.4$ (Fig. 13). With a LOC linewidth of 13.7 kHz the linewidth of the dual-cavity OPO is $\Delta\nu_{\mathrm{OPO}} = 5.5$ kHz in 20 μs. The uncertainty for the estimation of the parameter b is well below ± 0.1 and dominates the uncertainty of the OPOs linewidth fits (relative error $< 15\%$). The small difference between the two OPO types may be explained by the different mechanical cavity properties. As these linewidth values may contain a contribution from LOC length fluctuations, they represent an upper limit for both PR-SROs.

4 Conclusion

We have presented an analysis of the frequency stability of two PR-SRO devices on three different time scales. For both setups, a common-cavity and a dual-cavity PR-SRO design, a stabilization is possible. The frequency behaviour of both designs can be explained by the stabilization methods used. The long-term (30 minutes) stability is better than the ± 30 MHz wavemeter accuracy. The common-cavity PR-SRO shows a jitter of 56 kHz over 1.8 seconds, whereas for the dual-cavity system the frequency jitter is 13.5 MHz over 1.5 seconds. The linewidth for both OPOs is well below 10 kHz (relative error $< 15\%$) in 20 μs. The dual-cavity PR-SRO not only exhibits very good tunability [13], but also meets requirements on frequency stability and linewidth without using an external reference. In particular, it is suitable for efficient excitation of a high-finesse cavity in CALOS trace gas measurements. We have demonstrated that cw OPOs are a practical and flexible way to transfer the very narrow linewidth of a (fixed-wavelength) pump laser to a tunable wave. This opens up interesting perspectives for high-resolution spectroscopy, e.g., in the emerging field of ultracold molecules.

ACKNOWLEDGEMENTS We are grateful to the Deutsche Forschungsgemeinschaft for funding, to A. Peters (Humboldt Universität Berlin) for providing OPO optics and to K. Buse (Universität Bonn) for lending us a wavemeter. Part of this work was performed in the framework of the EU Network ‘‘Ultracold Molecules” (HPRN-CT-2002-00290).

REFERENCES

1 M. Ebrahimzadeh, M.H. Dunn: *Handbook of Optics IV*, M. Bass, J.M. Enoch, E.W. van Stryland, W.L. Wolfe, Eds. (McGraw-Hill, 2000), pp. 2201–2272
2 S. Schiller: *Encyclopedia of Modern Optics*, ed. by B. Guenther, D. Steel, L. Bayvel, Vol. 4 (Elsevier 2004) pp. 51–62
3 C. Wunderlich, C. Balzer: Adv. At., Mol., Opt. Phys. **49**, 293 (2003)
4 M.W. Sigrist: Rev. Sci. Instrum. **74**, 486 (2003)
5 F. Tittel, D. Richter, A. Fried: Topics Appl. Phys. **89**, 445 (2003)
6 A. Hecker, M. Havenith, C. Braxmaier, U. Strößner, A. Peters: Opt. Comm. **218**, 131 (2003)
7 M. M. J. W. v. Herpen, S. Li, S.E. Bisson, S. Te Lintel Hekkert, F.J.M. Harren: Appl. Phys. B **75**, 329 (2002)
8 M. M. J. W. v. Herpen, S.E. Bisson, A.K.Y. Ngai, F.J.M. Harren: Appl. Phys. B **78**, 281 (2004)
9 E.V. Kovalchuk, D. Dekorsy, A.I. Lvovsky, C. Braxmaier, J. Mlynek, A. Peters, S. Schiller: Opt. Lett. **26**, 1430 (2001)
10 A. Popp, F. Müller, F. Kühnemann, S. Schiller, G. v. Basum, H. Dahnke, P. Hering, M. Mürtz: Appl. Phys. B **75**, 751 (2002)
11 G. v. Basum, D. Halmer, P. Hering, M. Mürtz, S. Schiller, F. Müller, A. Popp, F. Kühnemann: Opt. Lett. **29**, 797 (2004)
12 F. Kühnemann, K. Schneider, A. Hecker, A.A.E. Martis, W. Urban, S. Schiller, J. Mlynek: Appl. Phys. B **66**, 741 (1998)
13 F. Müller, A. Popp, F. Kühnemann, S. Schiller: Optics Express **11**, 2820 (2003)
14 F. Kühnemann: *Laser in Environmental and Life Science*, P. Hering, J.P. Lay, S. Stry, Eds. (Springer, Heidelberg-Berlin, 2003), Chapt. 16
15 D. Romanini, A.A. Kachanov, N. Sadeghi, F. Stoeckel: Chem. Phys. Lett **264**, 316 (1997)
16 B.A. Paldus, C.C. Harb, T.G. Spence, R.N. Zare, C. Gmachl, F. Capasso, D.L. Sivco, J.N. Baillargeon, A.L. Hutchinson, A.Y. Cho: Opt. Lett. **25**, 666 (2000)
17 S. Schiller, V. Korobov: to appear in Phys. Rev. A
18 R. Al-Tahtamouni, K. Bencheikh, R. Storz. K. Schneider, M. Lang, J. Mlynek, S. Schiller: Appl. Phys. B **66**, 733 (1998)
19 U. Strößner, J.-P. Meyn, R. Wallenstein, P. Urenski, A. Arie, G. Rosenman, J. Mlynek, S. Schiller, A. Peters: J. Opt. Soc. Am. B **19**, 1419 (2002).
20 Z. Li, R.G.T. Bennett, G.E. Stedman: Opt. Comm. **86**, 51 (1991)
21 T.J. Kane, A.C. Nilsson, R.L. Byer: Opt. Lett. **12**, 175 (1987)
22 L.E. Myers, R.C. Eckardt, M.M. Fejer, R.L. Byer, W.R. Bosenberg, J.W. Pierce: Opt. Lett. **21**, 591 (1996)

23 M.E. Klein, D.-H. Lee, J.-P. Meyn, K.-J. Boller, R. Wallenstein: Opt. Lett. **24**, 1142 (1999)
24 F.G. Colville, M.J. Padgett, M.H. Dunn: Appl. Phys. Lett. **64**, 1490 (1994)
25 A.J. Henderson, P.M. Roper, L.A. Borchowa, R.D. Mead: Opt. Lett. **25**, 1264 (2000)
26 M. Martinelli, K.S. Zhang, T. Coudreau, A. Maitre, C. Fabre: J. Opt. A **3**, 300 (2001)
27 K. Schneider, P. Kramper, S .Schiller, J. Mlynek: Opt. Lett. **22**, 1293 (1997)
28 G. Turnbull, D. McGloin, I. Lindsay, M. Ebrahimzadeh, M. Dunn: Opt. Lett. **25**, 341 (2000)
29 D.J.M. Stothard, I.D. Lindsay, M.H. Dunn: Optics Express **12**, 502 (2004)
30 R.W.P. Drever, J.L. Hall, F.V. Kowalski, J. Hough, G.M. Ford, A.J. Munley, H. Ward: Appl. Phys. B **31**, 97 (1983)